



Prognostic value of inflammation and immune-related gene NOD2 in clear cell renal cell carcinoma

Lei Lyu¹ · Rui Min¹ · Fuxin Zheng¹ · Wei Xiang¹ · Tao Huang¹ · Yan Feng² · Chuanhua Zhang¹ · Jingdong Yuan¹

Received: 29 June 2023 / Accepted: 16 February 2024 / Published online: 21 March 2024
© The Author(s) under exclusive licence to Japan Human Cell Society 2024

Abstract

Inflammation and immune responses play important roles in cancer development and prognosis. We identified 59 upregulated inflammation- and immune-related genes (IIRGs) in clear cell renal cell carcinoma (ccRCC) from The Cancer Genome Atlas database. Among the upregulated IIRGs, nucleotide binding oligomerization domain 2 (NOD2), PYD and CARD domain (PYCARD) were also confirmed to be upregulated in the OncoPrint database and in three independent GEO data sets. Tumor immune infiltration resource database analysis revealed that NOD2 and PYCARD levels were significantly positively correlated with infiltration levels of B cells, CD4+ T cells, CD8+ T cells, neutrophils, macrophages and dendritic cells. Multivariate Cox hazards regression analysis indicated that based on clinical variables (age, gender, tumor grade, pathological TNM stage), NOD2, but not PYCARD, was an independent, unfavorable ccRCC prognostic biomarker. Functional enrichment analyses (GSEA) showed that NOD2 was involved in innate immune responses, inflammatory responses, and regulation of cytokine secretion. Meanwhile, mRNA and protein levels of NOD2 were elevated in four ccRCC cell lines (786-O, ACHN, A498 and Caki-1), and its knockdown significantly inhibited IL-8 secretion, thereby inhibiting ccRCC cell proliferation and invasion. Furthermore, results showed that miR-20b-5p targeted NOD2 to alleviate NOD2-mediated IL-8 secretion. In conclusion, NOD2 is a potential prognostic biomarker for ccRCC and the miR-20b-5p/NOD2/IL-8 axis may regulate inflammation- and immune-mediated tumorigenesis in ccRCC.

Keywords Clear cell renal cell carcinoma · Inflammation · Immune · Prognosis · NOD2

Introduction

Clear cell renal cell carcinoma (ccRCC) is the most common malignant tumor of the kidney, accounting for 70% of all kidney tumors [1]. Despite advances in ccRCC diagnosis

and treatment, 30% of localized ccRCC patients experience recurrence or metastasis, while 30% of them have advanced or metastatic renal cell carcinoma (mRCC) at initial diagnosis [2]. Patients with advanced ccRCC have poor prognostic outcomes, with a 5-year survival rate being less than 10% [3].

ccRCC is not sensitive to traditional chemoradiotherapy and exhibit typical intratumoral heterogeneity, which increases the unpredictability of its clinical progression [4]. Development of molecular targeted drugs, including tyrosine kinase inhibitors (TKIs) and mammalian target of rapamycin (mTOR) inhibitors has significantly improved the prognostic outcomes of patients with advanced ccRCC [5]. In the past 10 years, the median overall survival (OS) has been extended from 13 to 30 months, which is a milestone in the treatment of advanced ccRCC [6, 7]. However, targeted therapy has various limitations such as drug resistance, side effects or toxicity, which limits its clinical benefits among high-risk groups for ccRCC [8]. Therefore, there is a need to develop new treatment

Lei Lyu, Rui Min and Fuxin Zheng have contributed equally to this work as co-first authors.

✉ Jingdong Yuan
YuanJD97@163.com

¹ Department of Urology, Wuhan No.1 Hospital (Traditional Chinese and Western Medicine Hospital of Wuhan), Tongji Medical College, Huazhong University of Science and Technology, Hubei, Wuhan 430022, People's Republic of China

² Department of Pathology Wuhan No.1 Hospital (Traditional Chinese and Western Medicine Hospital of Wuhan), Tongji Medical College, Huazhong University of Science and Technology, Hubei, Wuhan 430022, People's Republic of China

methods to further improve the prognostic outcomes of advanced ccRCC patients.

Immune checkpoint inhibitors (ICIs), such as programmed cell death-1 (PD-1), programmed cell death ligand-1 (PDL-1) and cytotoxic T lymphocyte-associated antigen-4 (CTLA-4) have revolutionized the treatment of advanced ccRCC patients [9, 10]. For patients who do not benefit from traditional molecular targeted therapy, ICIs have shown the prognostic outcomes and prolonged their survival time, suggesting that immunotherapy is effective for ccRCC treatment [11]. Thus, screening and identification of novel immune related genes (IRGs) is a research hotspot in ccRCC prevention and treatment. For instance, Pan et al. reported that as an immune-related gene (IRG), Layilin (LYAN) can predict immune infiltrations and prognostic outcomes of gastric and colon cancers [12]. Wang et al. reported that as a potential IRG, scavenger receptor class A member 5 (SCARA5) affects the proliferation and migration of triple-negative breast cancer (TNBC) cells, indicating that SCARA5 may be a potential immunotherapeutic target for TNBC [13]. However, the clinical significance of these IRGs and functionally important genes have not been clarified in large clinical cohorts. Therefore, it is important to identify valuable IRGs using large clinical samples and to investigate the biological mechanisms involved in ccRCC development.

Various inflammatory factors (chemokines, cytokines and small inflammatory proteins) as well as immune-related cells interact during carcinogenesis and metastasis [14, 15]. In the tumor microenvironment, abnormal dynamic changes between inflammation and immunity lead to inflammation induced-immunosuppression and mediated-immune escape. Weber et al. reported that IL-6 is an important regulator of myeloid-derived suppressor cell (MDSC) activities and a potential target for cancer immunotherapy [16]. Evidence has revealed that FGF2 regulates macrophage polarization and tumor immunity as well as proliferation in the tumor microenvironment [17]. However, the roles and interaction mechanisms for inflammation and immune cells have not been fully elucidated.

In this study, to investigate the effects of inflammation and immune regulation on the prognosis of ccRCC and its underlying mechanism, we performed bioinformatics analyses using public clinical cohorts. A total of 59 differentially expressed inflammation-and immune-related genes (IIRGs) were identified in ccRCC. We identified NOD2 to be a novel IIRG for ccRCC diagnosis and prognosis. Moreover, over-expression of NOD2 in ccRCC cells promoted cancer cell proliferation and invasion by inducing IL-8 secretion. Meanwhile, miR-20b-5p blocked NOD2-mediated IL-8 secretion, thereby inhibiting ccRCC cell proliferation and invasion.

Materials and methods

Database

The RNA expression profiles (level 3 RNA-seq 2 data) and clinical data of 537 ccRCC patients (including 537 ccRCC tissue samples and 72 normal renal tissue samples) were downloaded from the Cancer Genome Atlas (TCGA) database (<https://portal.gdc.cancer.gov/>) in June 2021. The clinical information of ccRCC patients is presented in Table 1.

Functional enrichment analysis

To investigate the potential biological mechanisms of the inflammation- and immune-related prognostic signature, the ccRCC expression data from the TCGA database were subjected to Gene Set Enrichment Analysis (<http://www.gsea-msigdb.org/gsea/index.jsp>) using the immunologic signature gene set (c7.all.v7.4.symbols.gmt) and hallmark gene sets (h.all.v7.4.symbols.gmt). $P \leq 0.05$ was set as the threshold for statistical significance. In addition, GO database (<http://www.geneontology.org>) and the Kyoto

Table 1 Clinical characteristic of ccRCC patients from TCGA

Characteristics	Patients	
	<i>n</i> = 537	%
Age(years)		
≤60	266	49.5
>60	271	50.5
Gender		
Male	346	64.4
Female	191	35.6
Tumor grade		
G1–G2	244	45.4
G3–G4	285	53.1
Unkown	8	1.5
TNM staging system		
T1–T2	344	64.1
T3–T4	193	35.9
TNM staging system		
N0	240	44.7
N1	17	3.2
Nx	280	52.1
TNM staging system		
M0	426	79.3
M1	79	14.7
Mx	32	6.0
Status		
Survival	367	68.3
Death	170	31.7

Encyclopedia of Genes and Genomes (KEGG) database (<http://www.kegg.jp>) were used to perform functional annotations (biological process (BPs), cellular components (CCs) and molecular functions (MFs)) of differentially expressed IIRGs. Relationships among enriched clusters in GO and KEGG signaling pathways were visualized using Metascape (<http://www.metascape.org/>) and GeneMANIA (<http://genemania.org>).

Expression of IIRGs

Through GSEA, differentially expressed IIRGs in ccRCC tissues were identified using “limma” in R [$P < 0.05$, log₂ fold change (logFC) > 1.0 , FDR < 0.01]. The Oncomine gene expression microarray (<https://www.oncomine.org>) datasets were used to verify IIRGs levels in ccRCC. Three independent microarray data sets (GSE40435, GSE53757, and GSE66272) were downloaded from the Gene Expression Omnibus (GEO) database (<https://www.ncbi.nlm.nih.gov/geo/>) for validation. The association between IIRGs and clinical characteristics of ccRCC patients were also analyzed.

Survival analysis and univariate and multivariate Cox proportional hazards regression analyses

Through the online database, Gene Expression Profiling Interactive Analysis (GEPIA2) (<http://gepia2.cancer-pku.cn>), Kaplan–Meier survival curves were developed to evaluate the prognostic significance of IIRGs. For overall survival (OS) analyses, ccRCC patients were assigned into two groups based on median expressions of mRNAs (high vs. low). Survival curves for samples with low and high mRNA expressions were compared using the log-rank test. Next, univariate and multivariate Cox proportional hazards regression analyses were performed to determine NOD2 and PYCARD levels as well as clinical features (age, gender, grade, pathologic TNM stage) that were significantly associated with OS. $P \leq 0.05$ was set as the threshold for statistical significance.

cBioPortal analysis

Genomic profiles, including the frequencies of NOD2 and PYCARD alterations (mutation, amplification, and multiple alterations), putative copy number variations (CNVs) as well as mRNA expression levels of NOD2 and PYCARD were obtained from genomic identification of significant targets in cancer (GISTIC). Correlation between gene expression and DNA methylation as well as co-expression was analyzed according to cBioPortal’s online instructions (<http://www.cbioportal.org/>).

Correlations between NOD2 and PYCARD levels with the abundance of immune infiltrates in ccRCC

Using ccRCC expression data in the TCGA database, correlation between NOD2 and PYCARD levels and immune infiltration (including B cells, CD4+ T cells, CD8+ T cells, macrophages, dendritic cells) in ccRCC was evaluated using the tumor immune infiltration resource (TIMER) database (<http://timer.cistrome.org/>). Association of NOD2 and PYCARD levels with gene markers of tumor-infiltrating immune cells was evaluated by the Spearman’s correlation analysis. Gene expression levels corrected for tumor purity were used to estimate infiltrations.

Cell cultures

The human renal tubular epithelial cell line (HK-2) and four human ccRCC cell lines (786-O, ACHN, A498 and Caki-1) were purchased from the American Type Culture Collection (ATCC, Manassas, VA, United States) and cultured in DMEM medium supplemented with 10% Fetal bovine serum (Thermo Scientific HyClone, Logan, UT, United States).

RNA interference

The mRNA sequence of NOD2 was obtained from GenBank (NM_022162). For RNA interference, targeting sequences were designed using an online RNAi algorithm (<http://sidirect2.rnai.jp/>). The three NOD2-specific siRNAs (si-NOD2 #1: 5'-AGACAAAGAGAAAUCCUGGA-3', si-NOD2 #2: 5'-GCCUGAUGUUGGUCAAGAAGA-3', si-NOD2 #3: 5'-AACCUUUGAUGGCUUUGA CGA-3') and a negative control siRNA (NC siRNA) were purchased from GenePharma (Shanghai, China). The 786-O and ACHN cells were transfected with Translipid reagent (TransGen, Beijing, China) following the manufacturer’s instructions.

Quantitative real-time PCR (qRT-PCR)

Total RNA was extracted using the Trizol Reagent (Invitrogen, Carlsbad, CA, United States) and there after reverse transcribed into cDNA using a reverse transcription kit (TransGen, Beijing, China). Quantitative real time polymerase chain reaction (qRT-PCR) analysis was performed to assess relative expressions of target gene RNA. Sequences for the specific primers were; 5'-TGGTTCAGCCTCTCA CGATGA-3' (Forward) and 5'-CAGGACACTCTCGAA GCCTT-3' (Reverse) for NOD2; 5'-TGAAGGTCGGAG TCAACGG-3' (Forward) and 5'-CCTGGAAGATG GTG ATGGG-3' (Reverse) for GAPDH; 5'-CTCGCTTCGGCA GCACA-3' (Forward) and 5'-AACGCTTACGAATTTGC GT-3' (Reverse) for U6; 5'-ACACTCCAGCTGGGCGCT TTGCT CAGCCA-3' (Forward) for miR-1251-3p; 5'-ACA

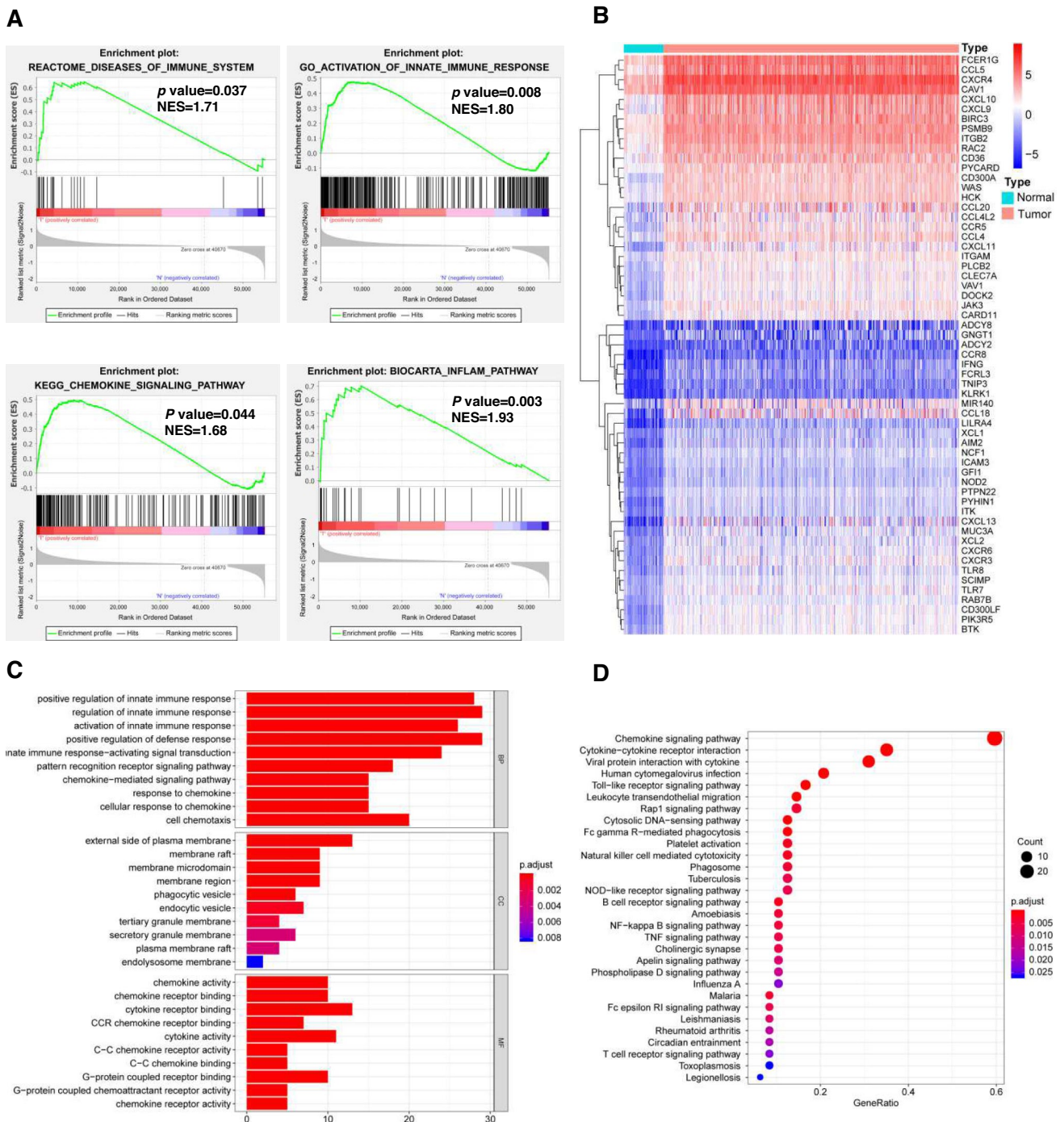


Fig. 1 Differentially expressed IIRGs and functional annotations. **a** Inflammation and immune-related pathways identified through GSEA analysis. **b** Heatmap of the 59 upregulated IIRGs in 72 normal renal

tissue samples and 537 ccRCC tissue samples. **c** GO enrichment analysis of the 59 upregulated IIRGs. **d** KEGG pathway enrichment analysis of the 59 upregulated IIRGs

CTCCAGCTGGGTAAGG CACGCGGU GAA-3' (Forward) for miR-124-3p; 5'-ACACTCCAGCTGGGCAAAGTGCTC ATAGT-3' (Forward) for miR-20b-5p. All reverse primers for miRNAs were universal 3' miRNA primers 5'-TGGTGT

CGTGGAGTCG-3'. GAPDH and U6 were the internal controls. Relative RNA expressions were calculated using the $2^{-\Delta\Delta C_T}$ method.

Western blotting

Protein extractions from cells was performed using the RIPA lysis buffer (Thermo Fisher Scientific, Waltham, MA, United States). Then, proteins were quantified using the bicinchoninic acid (BCA) method, resolved by 12% SDS-PAGE, electro-transferred to polyvinylidene difluoride (PVDF) membranes, which were subsequently blocked using 5% skim milk, incubated at 4°C overnight in the presence of primary antibodies against NOD2 or GAPDH (Abcam, Cambridge, UK), followed by incubation with secondary antibodies (Antgene, Wuhan, China) at room temperature for 30 min. Blots were detected by chemiluminescence (Pierce, Thermo Fisher Scientific, United States).

3-(4,5)-dimethylthiazol(-2-yl)-3,5-diphenyltetrazolium bromide (MTT) assay and 5-ethynyl-2'-deoxyuridine (EdU) assay

Cells were seeded in 96-well plates (5×10^3 cells/well) and incubated for the indicated duration. Absorbance was detected at 490 nm and cell viabilities evaluated via the MTT assay (Beyotime Biotechnology, Shanghai, China), as instructed by the manufacturer. Cell proliferation viabilities were also assessed by the EdU assay (RiboBio, Guangzhou, China). Briefly, 5×10^3 cells were seeded in each well of 96-well plates and pretreated for the indicated time. Next, cells were incubated with the EdU reagent (50 μ M) for 30 min at 37 °C. Subsequently, they were fixed with 4% formaldehyde and incubated with 100 μ l of reaction cocktail for 30 min. The DNA content of the cells in each well was stained with DAPI for 10 min and visualized by fluorescence microscopy. Positive cells fluoresced red while their nucleus fluoresced blue after DAPI staining. Cell proliferation levels in each group were compared to those of the control group.

Invasion assay

Pretreated cells were seeded in the upper chamber of a culture plate with 8 μ m pore matrigel-coated polycarbonate membranes (Costar, United States) (2×10^5 /per well) and there after incubated. The upper chamber contained serum-free DMEM medium while the lower chamber was filled with 10%-FBS-supplemented DMEM. After 24 h of incubation, invading cells at the bottom of the polycarbonate membrane were fixed and stained with crystal violet. The number of invading cells in at least three random fields was counted.

Enzyme-linked immunosorbent assay (ELISA)

Cells were seeded in 6-well plates (1×10^6 cells/well) and incubated for 48 h. Then, cell supernatants were obtained

by centrifugation (1000 \times g, 10 min, 4 °C) and used for the ELISA assay (Beyotime Biotechnology, Shanghai, China) to assess cytokine levels. Briefly, standards and diluted samples were added to 96-well ELISA plates and incubated at 37 °C for 120 min. The plates were washed and biotinylated antibodies were added to each well and incubated for 60 min. Subsequently, horseradish peroxidase-labeled streptavidin complex was added to each well and incubated for 60 min. Finally, tetramethylbenzidine (TMB) substrate was added for color development. The absorbance values at 450 nm were detected using an ELISA microplate reader.

Clinical samples

12 pairs of ccRCC and paracancerous tissue samples were obtained from ccRCC patients who underwent surgery in Wuhan No.1 Hospital. All patients underwent histopathological diagnosis and did not receive any local or systemic treatment prior to surgery. The clinical information of ccRCC patients is shown in Table S1. The tissues were promptly frozen in liquid nitrogen and subsequently stored at a temperature of – 80 °C. Written informed consent was obtained from all patients, and was in accordance with the Declaration of Helsinki. This study was approved by the Ethical Board of Wuhan No.1 Hospital, Tongji Medical College, Huazhong University of Science and Technology with written informed consent from all the patients (Ethics Approval Number: 2020IECA255).

Immunohistochemistry (IHC)

Immunohistochemistry (IHC) was performed to measure the protein levels of NOD2, IL-2 and IL-8 (Abcam, Cambridge, UK) in 12 pairs ccRCC and paracancerous tissues using the avidin–biotin–peroxidase complex (ABC) technique. The sectioning procedure was performed by two skilled pathologists, who carefully identified and chose the renal cortex region characterized by an abundance of proximal tubules. Subsequently, immunohistochemical analysis was performed, followed by comprehensive labeling and description. Images were acquired with an Olympus microscope (Olympus, Japan).

Luciferase reporter gene assay

Wild-type or mutant NOD2 3'-UTR region sequences were amplified and cloned into the luciferase reporter vector, pmiR-Report (Promega, Madison, WI, United States). After co-transfections with these plasmids and miRNA mimics for 48 h, ccRCC cells were harvested via passive lysis buffer (Promega). Relative luciferase activities were assayed by the

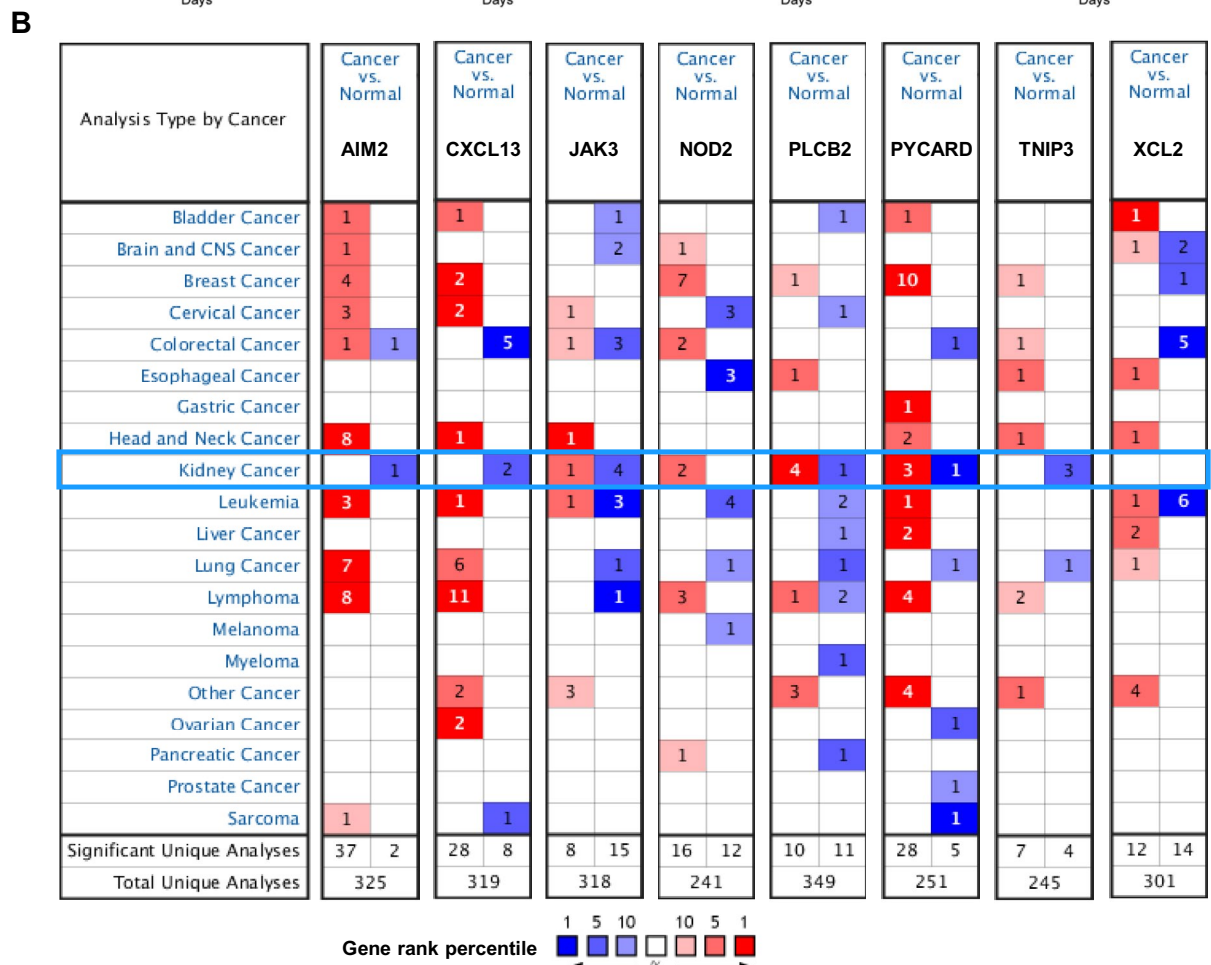
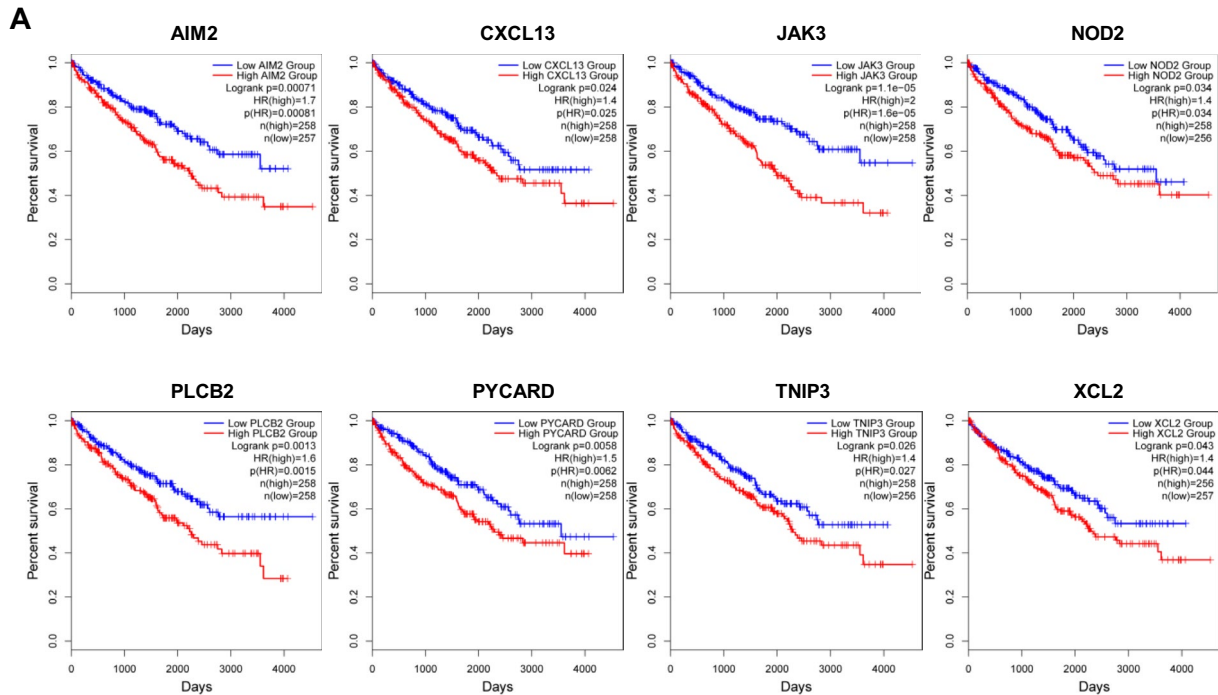


Fig. 2 Expression levels of 8 prognosis-related IIRGs in ccRCC patients. **a** Kaplan–Meier survival analysis showing the relationship between IIRG levels and prognostic outcomes in ccRCC patients using the GEPIA database. Survival curve of the 8 prognosis-related IIRGs. **b** Expression of 8 prognosis-related IIRGs in Oncomine databases

dual luciferase reporter system (Promega) and normalized to the luciferase activity of Renilla.

RNA immunoprecipitation (RIP) experiments

RNA immunoprecipitation (RIP) experiments were performed using the EZ-Magna RIP™ RNA-Binding Protein Immunoprecipitation kit (Millipore, Billerica, MA, USA). In summary, the ccRCC cells were collected and disrupted in RIP lysis buffer as per the guidelines provided by the manufacturer. Following this, pre-incubated magnetic beads that were coated with specific antibodies were utilized to immunoprecipitate the supernatant of the cell lysate for a duration of 6 h at a temperature of 4 °C. Subsequently, the purified RNA was assessed using RT-qPCR.

Statistics

Data are presented as means \pm SD. The SPSS 22.0 software (SPSS Inc., Chicago, IL, United States) was used for data analyses. Comparisons of means between and among groups were performed by the independent samples *t* test and one-way ANOVA, respectively. The Kaplan–Meier method and log-rank test were used for survival analyses. Risk factors for prognosis were evaluated by univariate and multivariate Cox regression analysis, and correlation analyses performed by the Spearman method. $P \leq 0.05$ denoted significant differences. In vitro experiment, data are representative images or expressed as the mean \pm SD of each group from three independent experiments.

Results

Differentially expressed IIRGs in ccRCC

First, we performed GSEA using REACTOME, KEGG, GO and BIOCARTA databases to confirm whether ccRCC development is associated with inflammation and immunity. It was established that the immune system, innate immune response activations, chemokine signaling pathway and inflammatory pathway were closely associated with tumorigenesis and ccRCC development (Fig. 1a). A total of 223 IIRGs were found based on the results of GSEA, among which 59 were significantly upregulated (none of the IIRGs were significantly

downregulated) (Fig. 1b, Fig. S1 and Table S2). Therefore, we further explored the roles of these significantly upregulated IIRGs. The GO plot analysis revealed that these IIRGs were enriched in regulation of innate immune responses as well as in cellular responses to chemokines (Fig. 1c). Significant KEGG pathways in which these upregulated IIRGs were enriched were the chemokine signaling pathway, T cell receptor signaling pathway, Toll-like receptor signaling pathway, NOD-like receptor signaling pathway and TNF signaling pathway (Fig. 1d), which identified the major roles of these upregulated IIRGs in ccRCC tumorigenesis and development.

Kaplan–Meier survival analyses of upregulated IIRGs

To investigate whether upregulated IIRGs were associated with prognostic outcomes, ccRCC patients were assigned into two groups (low group vs. high group) according to the median value of IIRGs levels, and each group was analyzed by Kaplan–Meier survival analysis using the GEPIA online database. Among the 59 upregulated IIRGs, 8 IIRGs (AIM2, CXCL13, JAK3, NOD2, PLCB2, PYCARD, TNIP3 and XCL2) were significantly negatively correlated with OS (Fig. 2a). Then, we validated the expression levels of these prognosis-related IIRGs in ccRCC and normal kidney tissues using the Oncomine database. Among the 8 prognostic-related IIRGs, only three (NOD2, PLCB2 and PYCARD) were upregulated in ccRCC (Fig. 2b). These three IIRGs from the Oncomine databases were further tested in three independent GEO data sets (GSE53757, GSE66272 and GSE40435) using GEO2R for verification (Table 2). The mRNA expressions of two prognosis-related IIRGs (NOD2 and PYCARD) in ccRCC were significantly upregulated, compared to those of normal kidney tissues, suggesting that NOD2 and PYCARD play important roles in ccRCC development. Subsequently, we investigated the biological roles of NOD2 and PYCARD in ccRCC.

Association between NOD2 or PYCARD mRNA levels and clinical features of ccRCC patients

To elucidate on the correlation between NOD2 or PYCARD levels and prognostic outcomes of ccRCC, subgroup analyses of ccRCC clinical features using the TCGA database were performed. The mRNA levels of NOD2 and PYCARD were significantly positively correlated with tumor grade and pathological TNM stage, but not significantly correlated with age and gender (Fig. 3a).

Table 2 Expression levels of NOD2, PLCB2 and PYCARD in ccRCC tissues in independent GEO databases

Gene symbol	Ensembl ID	GEO	Platform	Platform ID	Fold change	P value
NOD2	ENSG00000167207	GSE53757	GPL570	220066_at	3.89	1.03E-20
		GSE66272			7.94	4.28E-14
		GSE40435	GPL10558	ILMN_1762594	1.52	2.43E-30
PLCB2	ENSG00000137841	GSE53757	GPL570	210388_at	0.90	2.53E-01
		GSE66272			0.81	1.40E-01
		GSE40435	GPL10558	ILMN_1724066	1.86	1.64E-39
PYCARD	ENSG00000103490	GSE53757	GPL570	221666_s_at	4.57	4.08E-30
		GSE66272			6.48	6.73E-17
		GSE40435	GPL10558	ILMN_1698766	2.85	1.28E-45

Genomic alterations of NOD2 and PYCARD in ccRCC

Genomic alterations of NOD2 and PYCARD in ccRCC were evaluated using cBioPortal databases. NOD2 and PYCARD levels were altered in 26 (4.84%) and 29 (5.40%) of 537 ccRCC patients, respectively. For NOD2, the alterations included mutations in 5 cases (0.93%), mRNA upregulation in 8 cases (1.49%) and downregulation in 13 cases (2.42%), while multiple alterations were observed in 1 case (0.19%). Mutational sites for NOD2 were localized in the caspase recruitment domain (CARD) and NACHT domain. For PYCARD, the alterations included mutations in 2 cases (0.37%), amplification in 1 case (0.19%), mRNA upregulation in 12 cases (2.23%) and mRNA downregulation in 14 cases (2.61%). The mutation sites for PYCARD were located in the CARD and PAAD/DAPIN/Pyrin (PYRIN) domain (Fig. 3b–d). Correlation analyses revealed that mRNA expression of NOD2 or PYCARD was significantly negatively correlated with methylation levels (Fig. 3e). Importantly, NOD2 mRNA levels were significantly positively correlated with PYCARD mRNA levels (Fig. 3f), indicating that NOD2 mRNA and PYCARD mRNA were co-expressed in ccRCC.

Correlations between NOD2 or PYCARD expressions and immunological microenvironments of ccRCC

Given that NOD2 and PYCARD were closely associated with ccRCC immunity, we determined whether NOD2 or PYCARD levels were correlated with immune infiltration levels in ccRCC using the TIMER database. The expression levels of NOD2 and PYCARD were positively correlated with immune and stromal cell infiltrations in immunological microenvironments of ccRCC (Fig. 4a). Moreover, NOD2 and PYCARD levels were significantly positively correlated with infiltrating levels of B cells, CD4+ T cells, CD8+ T cells, neutrophils, macrophages and dendritic cells (Fig. 4b). We also found that NOD2 and PYCARD levels were significantly correlated with

marker genes of immune cells, such as CD4+ T (Th1) cell markers (IFN- γ and CCR5), T cell exhaustion markers (PD-1 and CTLA4), Treg markers (CCR8 and FOXP3) and M2 macrophage markers (VSIG4 and CD163) (Table 3). Thus, NOD2 and PYCARD play vital roles in immune escape mechanisms of ccRCC.

Independence of the prognostic value of NOD2 and PYCARD from clinical variables

To determine whether NOD2 and PYCARD are independent prognostic factors in ccRCC, univariable and multivariable Cox regression analyses with NOD2, PYCARD and clinical characteristics (age, gender, tumor grade and pathological TNM stage) as covariates were performed. It was established that age, pathological T, pathological M and high NOD2 mRNA levels were independent and unfavorable factors for OS (Table 4 and Fig. S2). However, PYCARD mRNA levels were not significant independent prognostic factors for OS in multivariable Cox regression analysis. Our findings imply that NOD2 has a more important role in ccRCC development, relative to PYCARD. Therefore, we evaluated the biological roles of NOD2 in ccRCC.

Biological interaction network of NOD2

First, we confirmed the biological functions of NOD2 based on the GeneMANIA database. We established that NOD2 is associated with regulation of innate immune responses, inflammatory responses, NF-kappaB signaling and regulation of cytokine secretions (Fig. 5a). Then, we performed GSEA using the TCGA databases to predict the potential functions of NOD2 in ccRCC. The findings indicated that stratified expression levels of NOD2 maybe be involved with cytokine signaling in the immune system, inflammatory pathway, tumor necrosis factor receptor and IL6/JAK/STAT3 signaling (Fig. 5b). To validate the potential functions of NOD2, Pearson correlation analysis

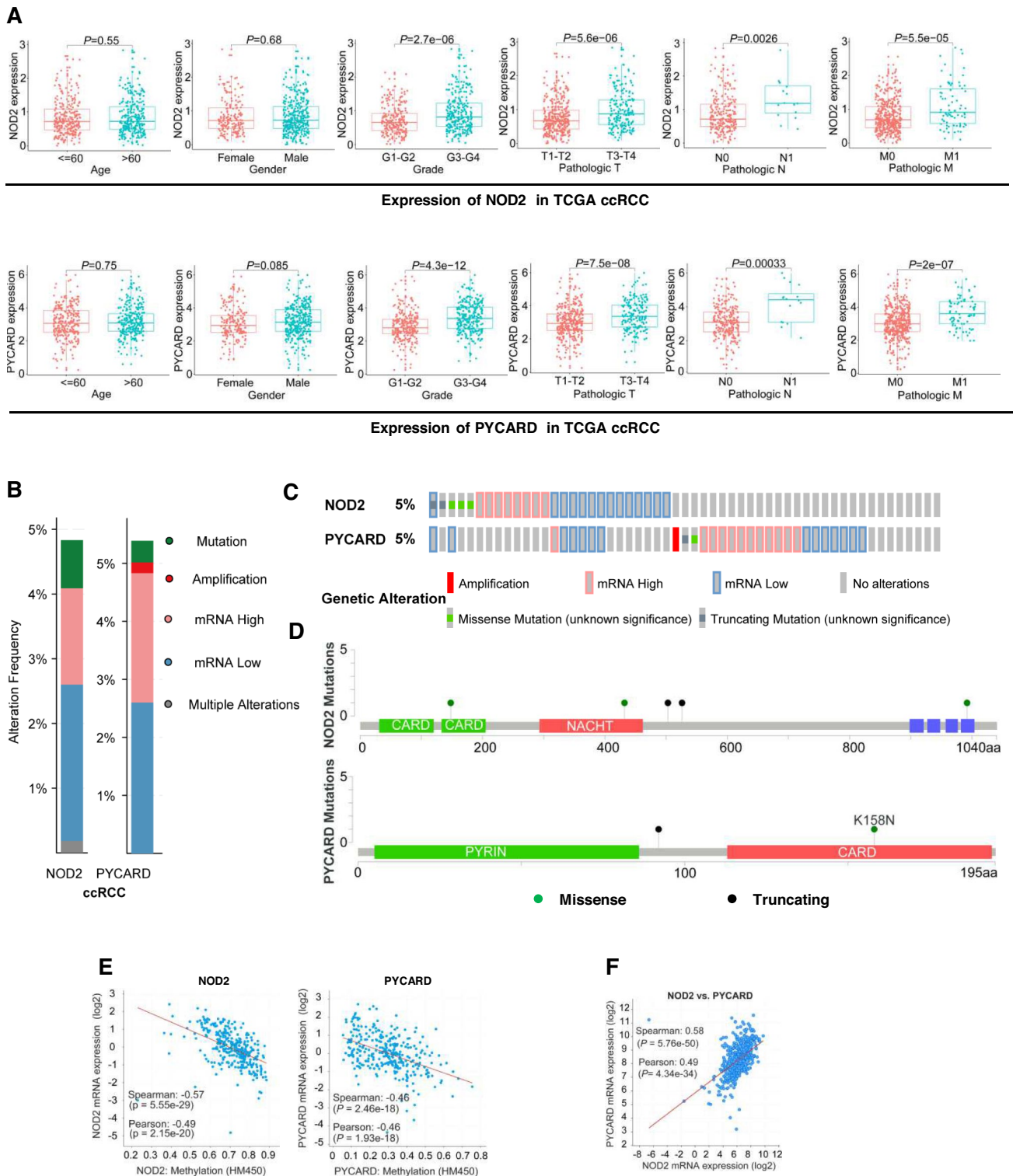


Fig. 3 mRNA expression and genomic alteration of NOD2 and PYCARD (cBioPortal). **a** Relative expression of NOD2 and PYCARD in subgroups of ccRCC samples stratified based on age, gender, tumor grade and pathological TNM stage. **b** Summary of alteration frequencies in NOD2 and PYCARD. **c** Distribution and

proportion of ccRCC samples with different types of alterations in NOD2 and PYCARD. **d** Mutational sites in NOD2 and PYCARD. **e** Correlation between NOD2 or PYCARD mRNA expression and methylation levels. **f** Correlation between mRNA expression of NOD2 and PYCARD

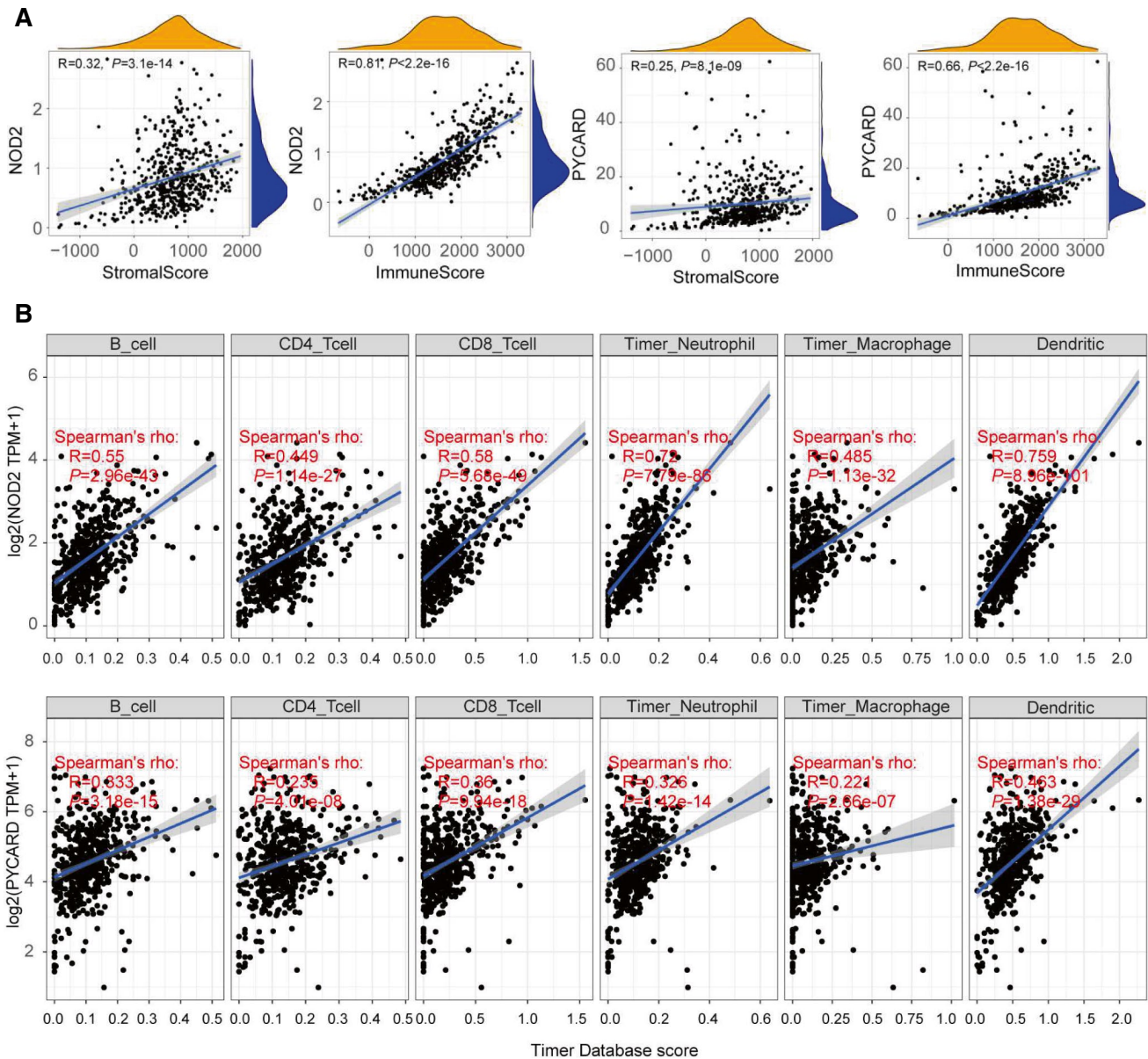


Fig. 4 Relationship between NOD2 or PYCARD expression and the immunological microenvironment (TIMER database). **a** Correlation between NOD2 or PYCARD with infiltration of immune and stromal

cells in ccRCC. **b** Correlations between NOD2 or PYCARD and infiltration levels of B cells, CD4+ T cells, CD8+ T cells, neutrophils, macrophages and dendritic cells

($|cor| \geq 0.4$, $FDR < 0.01$) was performed to construct the protein–protein co-expression interaction network. The 1202 protein-coding genes (PCGs) were significantly positively correlated with NOD2 (Top three PCGs: SNX20, GBP5 and VAV1), whereas 67 PCGs were significantly negatively correlated with NOD2 (Top three PCGs: CCNB1IP1, GLRX5 and BAG1). Enrichment analyses based on the results of Pearson correlation analysis were performed to further predict the potential biological functions of all PCGs that were correlated with NOD2. Consistent with GSEA

results, NOD2 was highly correlated with regulation of immune responses and cytokine production (Fig. 5c).

Effects of NOD2 on ccRCC proliferation and invasion

First, we validated NOD2 mRNA and protein levels in 4 ccRCC cell lines (786-O, ACHN, A498 and Caki-1) and in human proximal tubular cells (HK2) by qRT-PCR and Western blot, respectively. Compared to HK2 cells, mRNA and protein expressions of NOD2 in 4 ccRCC cell lines were significantly increased (Fig. 6a, b). The efficacy of individual

Table 3 Correlations between NOD2/PYCARD with related genes and immune cell markers in ccRCC

Immune cells	Gene markers	NOD2		PYCARD	
		Cor	<i>P</i> value	Cor	<i>P</i> value
B cell	CD19	0.464	***	0.468	***
	CD79A	0.491	***	0.493	***
CD4+ T cell (Th1)	STAT1	0.688	***	0.300	***
	IFN- γ (IFNG)	0.717	***	0.496	***
	CCR5	0.803	***	0.482	***
	TNF- α (TNF)	0.457	***	0.295	***
	GATA3	0.316	***	0.241	***
CD4+ T cell (Th2)	IL13	0.170	***	0.033	0.442
	STAT5A	0.634	***	0.424	***
	CD8A	0.694	***	0.491	***
CD8+ T cell	CD8B	0.659	***	0.532	***
	PD-1 (PDCD1)	0.728	***	0.597	***
T cell exhaustion	CTLA4	0.738	***	0.446	***
	CD305 (LAIR1)	0.744	***	0.536	***
Natural killer T cell	CD72	0.757	***	0.526	***
	CD94 (KLRC1)	0.394	***	0.365	***
	CD161 (KLRB1)	0.322	***	0.363	***
	CCR8	0.634	***	0.370	***
Treg	FOXP3	0.635	***	0.544	***
	TGF β (TGFB1)	0.165	***	0.140	*
	INOS (NOS2)	-0.026	0.542	-0.101	0.020
Macrophage (M1)	IRF5	0.573	***	0.383	***
	COX2 (PTGS2)	0.065	0.132	-0.133	0.213
	MS4A4A	0.501	***	0.283	***
Macrophage (M2)	VSIG4	0.529	***	0.403	***
	CD163	0.449	***	0.203	***
	CCR7	0.506	***	0.399	***
Neutrophils	CD44	0.416	***	0.317	***
	CD11b (ITGAM)	0.660	***	0.426	***
	HLA-DRA	0.682	***	0.410	***
Dendritic cell	HLA-DQB1	0.498	***	0.313	***
	BDCA-1 (CD1C)	0.298	***	0.226	***
	BDCA-4 (NRP1)	0.024	0.586	-0.280	***
	CD11C (ITGAX)	0.677	***	0.422	***

P* < 0.01, *P* < 0.001, ****P* < 0.0001**Table 4** Univariate and multivariate Cox regression analysis of OS outcomes for ccRCC patients

Variables	Univariate analysis			Multivariate analysis		
	HR	95% CI of HR	<i>P</i> value	HR	95% CI of HR	<i>P</i> value
Age($\leq 60 / > 60$)	1.748	1.278–2.390	<0.001	1.695	1.099–2.616	0.017
Gender (Male/Female)	1.060	0.773–1.454	0.719	0.868	0.562–1.339	0.521
Tumor grade (G1-G2/G3-G4)	2.628	1.851–3.733	<0.001	1.610	0.969–2.674	0.066
Pathological T (T1-T2/T3-T4)	3.406	2.492–4.654	<0.001	1.992	1.236–3.210	0.005
Pathological N (N0/N1)	3.196	1.699–6.012	<0.001	1.360	0.652–2.838	0.413
Pathological M (M0/M1)	4.329	3.146–5.959	<0.001	2.612	1.604–4.255	<0.001
NOD2 expression (Low/High)	1.552	1.372–1.756	<0.001	1.264	1.037–1.541	0.021
PYCARD expression (Low/High)	1.032	1.018–1.046	<0.001	1.004	0.980–1.028	0.767

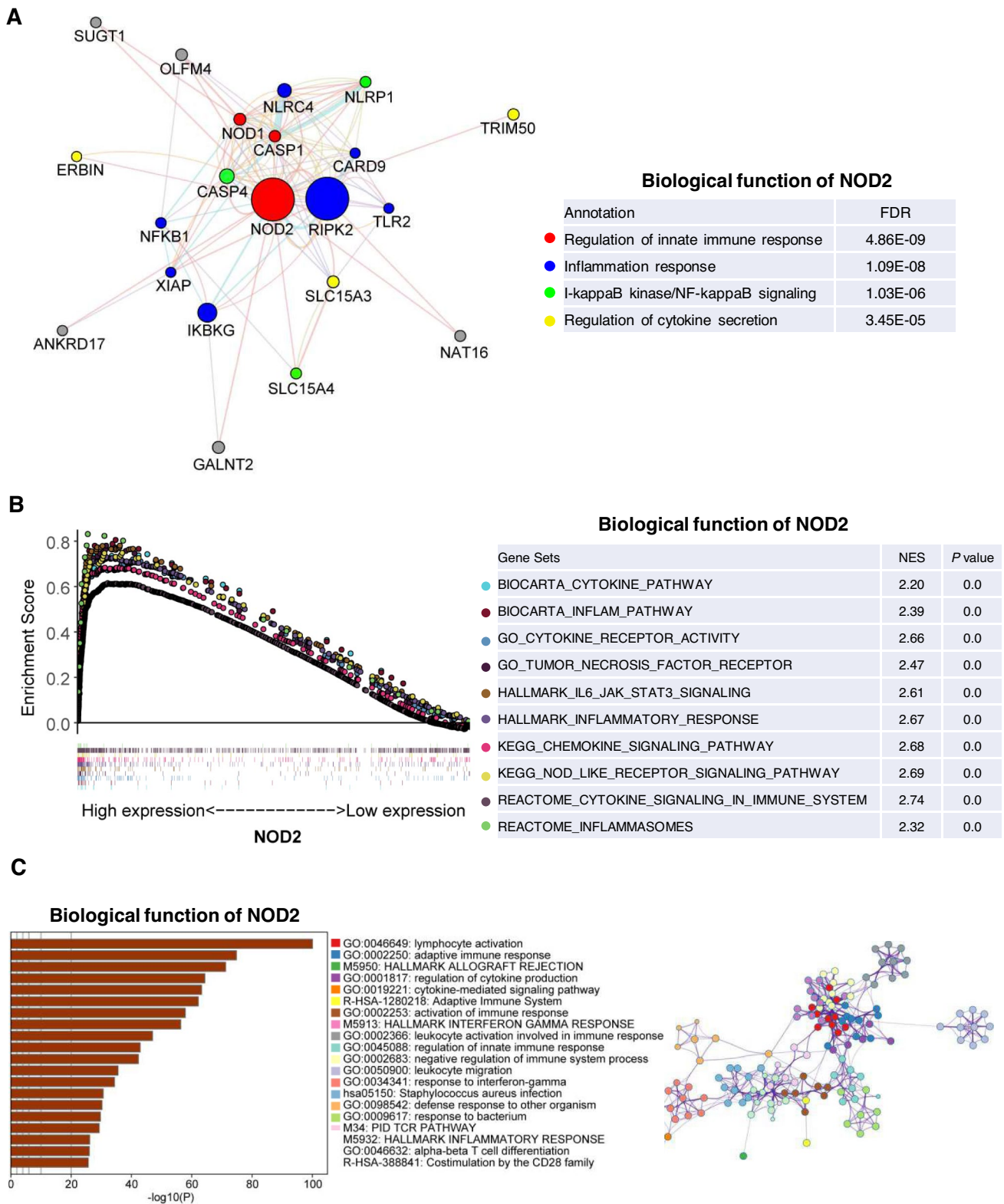


Fig. 5 Evaluation of the biological functions of NOD2. **a** GeneMANIA database analysis demonstrating interaction between the gene set and NOD2. **b** GSEA using stratified NOD2 expression levels for genes upregulated or downregulated in ccRCC. Correlation between NOD2 expression levels and their potential functions in

BIOCARTA, GO, HALLMARK, KEGG and REACTOM databases. **c** Enrichment analyses predicting the potential biological functions of the NOD2-related protein-coding genes (PCGs). Relationships among enriched clusters visualized with Metascape

inhibitory RNAs in down-regulating the expression of NOD2 gene was measured by qRT-PCR. The si-NOD2 #1 displayed the strongest inhibitory activity among these three NOD2 siRNAs tested. In the following study, we chose si-NOD2 #1 to investigate the effects of NOD2 knockdown on biological activities of ccRCC cells *in vitro* (Fig. S3). MTT (Fig. 6c), Edu (Fig. 6d) and invasion assay (Fig. 6e) results demonstrated that, compared with negative control siRNA (si-NC) group, NOD2 knockdown with NOD2 specific silencing RNA (si-NOD2 1# group) significantly inhibited 786-O cell and ACHN cell proliferation and invasion.

NOD2 induced secretion activation of IL-8

Since secretion activation of inflammatory cytokines play an important role in cancer development, we investigated whether NOD2 induced the release of inflammatory cytokines in 786-O cells and ACHN cells. First, we obtained culture medium supernatants and measured the expressions of cytokines that may be regulated by NOD2. Compared to HK-2 cells, IL-2 and IL-8 levels were significantly elevated in 786-O cells and ACHN cells (Fig. 6f). Meanwhile, immunohistochemistry (IHC) was performed to measure the protein levels of NOD2, IL-2 and IL-8 in human ccRCC tissues and their corresponding adjacent normal kidney tissues. The findings revealed a significant upregulation of NOD2, IL-2, and IL-8 expression in ccRCC tissues when compared to the adjacent normal kidney tissues (Fig. 6g). After transfections with NOD2 siRNA, IL-8 levels were significantly decreased in both cell types. However, IL-2 levels were not affected by NOD2 siRNA (Fig. 6h). These findings indicated that NOD2-induced IL-8 secretion may promote ccRCC cell invasion. To confirm whether IL-8 secretion activation could regulate the invasions of ccRCC cells, 786-O cells and ACHN cells were pretreated with an IL-8 antibody. Invasive abilities of 786-O and ACHN cells were significantly inhibited by the IL-8 antibody (Fig. 6i), suggesting that IL-8 secretion maybe responsible for NOD2-induced ccRCC cell invasions.

NOD2 is a direct target of miR-20b-5p

Considering that microRNAs regulate tumor development by modulating the expression and activity of specific mRNAs, we predicted miRNAs which may potentially target NOD2 using bioinformatics databases (miRDB, miRTarBase, TargetScan, and Starbase). Meanwhile, miRNAs downregulated in ccRCC were screened from the TCGA databases. Finally, 111 miRNAs targeting NOD2 and 114 miRNAs downregulated in ccRCC were identified, among which 3 miRNAs (miR-1251-3p, miR-124-3p and miR-20b-5p) were selected for overlapping prediction

analysis (Fig. 7a, b). In addition, the results of qRT-PCR test further confirmed that the expression levels of miR-124-3p and miR-20b-5p were lower in 4 ccRCC cell lines (786-O, ACHN, A498 and Caki-1) compared with levels in HK2 cells (Fig. 7c). Treatment with miR-20b-5p mimic downregulated the mRNA expression level of NOD2 in 786-O cells and ACHN cells indicating that NOD2 mRNA may be a potential target of miR-20b-5p (Fig. 7d, e). Meanwhile, we performed Pearson correlation analysis using TCGA databases to confirm that NOD2 mRNA expression level was significantly negatively correlated with the expression of miR-20b-5p (Fig. 7f). Subsequently, luciferase reporter cell lines carrying wild-type or mutant NOD2 3'-UTR regions were established to test whether NOD2 was a functional target of miR-20b-5p. The results revealed that cells co-transfected with miR-20b-5p mimic and wild-type NOD2 reporter vectors (NOD2-wt) had lower levels of the luciferase activity than cells co-transfected with negative control mimic (mimic NC) and NOD2-wt in 786-O cells and ACHN cells. However, mutation of the putative miR-20b-5p binding sites abolished these effects, indicating that NOD2 may be a potential target of miR-20b-5p (Fig. 7g, h). In order to conduct a more comprehensive investigation of the potential direct interaction between miR-20b-5p and NOD2, RNA immunoprecipitation (RIP) assays were performed on both 786-O cells and ACHN cells. The results demonstrated a clear immunoprecipitation of Ago2 protein from the extracts of both 786-O cells and ACHN cells. Additionally, the qRT-PCR analysis revealed a significantly higher enrichment of both miR-20b-5p and NOD2 in the Ago2 group when compared to the IgG group (Fig. S4A-4D).

miR-20b-5p inhibits ccRCC cell proliferation and invasion by blocking NOD2-mediated secretion activation of IL-8

The correlation between miR-20b-5p expression level and clinical features of ccRCC was explored in the TCGA database. It was observed that miR-20b-5p expression level was significantly negatively correlated with tumor grade and pathological TN stage, suggesting that miR-20b-5p influences the malignant degree and prognosis of ccRCC (Fig. 7i). We further explored whether the effects of miR-20b-5p were orchestrated through the NOD2-mediated IL-8 secretion. The results showed that overexpression of miR-20b-5p by miR-20b-5p mimic significantly inhibited IL-8 secretion, proliferation and invasion of 786-O cells and ACHN cells (Fig. 7j-1).

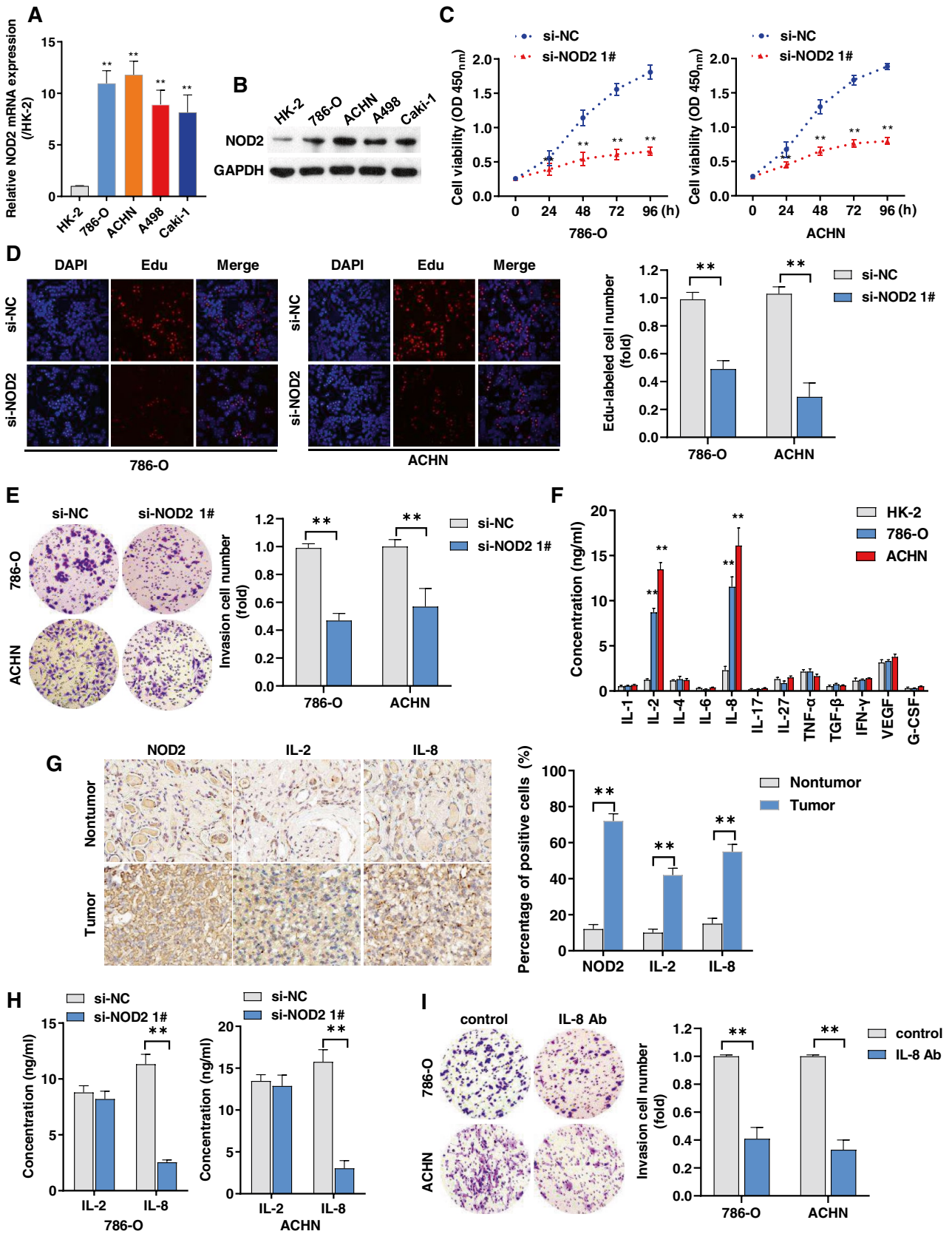


Fig. 6 Effects of NOD2 on ccRCC cell viability and invasion. **a, b** mRNA and protein levels of NOD2 in HK2 cells and four ccRCC cell lines (786-O, ACHN, A498 and Caki-1) detected by qRT-PCR and western blot, respectively. $**P < 0.05$ vs. HK2 cells. **c** 786-O and ACHN cells were transfected with negative control siRNA (si-NC) or NOD2-specific siRNA (si-NOD2 1#) for the indicated periods and cell viability was determined by the MTT assay. $**P < 0.05$ vs. the si-NC group. **d, e** 786-O and ACHN cells were transfected with si-NC or si-NOD2 1# for 48 h, EdU and invasion assays to evaluate proliferation and invasion, respectively. $**P < 0.05$ vs. si-NC group. **f** 786-O and ACHN cells were incubated for 48 h and cytokine levels in cell supernatants were analyzed by the ELISA assay. $**P < 0.05$ vs. HK2 cells. **g** 12 pairs of ccRCC and paracancerous tissue samples were obtained from ccRCC patients who underwent surgery. IHC were performed to analyze the protein expression levels of NOD2, IL-2 and IL-6 in normal renal proximal tubular epithelial cells and ccRCC. $**P < 0.05$ vs. Nontumor. **h, i** 786-O and ACHN cells were transfected with si-NC or si-NOD2 1# for 48 h, IL-2 and IL-8 levels in cell supernatants were determined by ELISA, while invasion viability were assessed by the invasion assay. $**P < 0.05$ vs. si-NC group or control group. In vitro experiment, data are representative images or expressed as the mean \pm SD of each group of cells from three independent experiments. Representative images are shown at $\times 100$ magnification

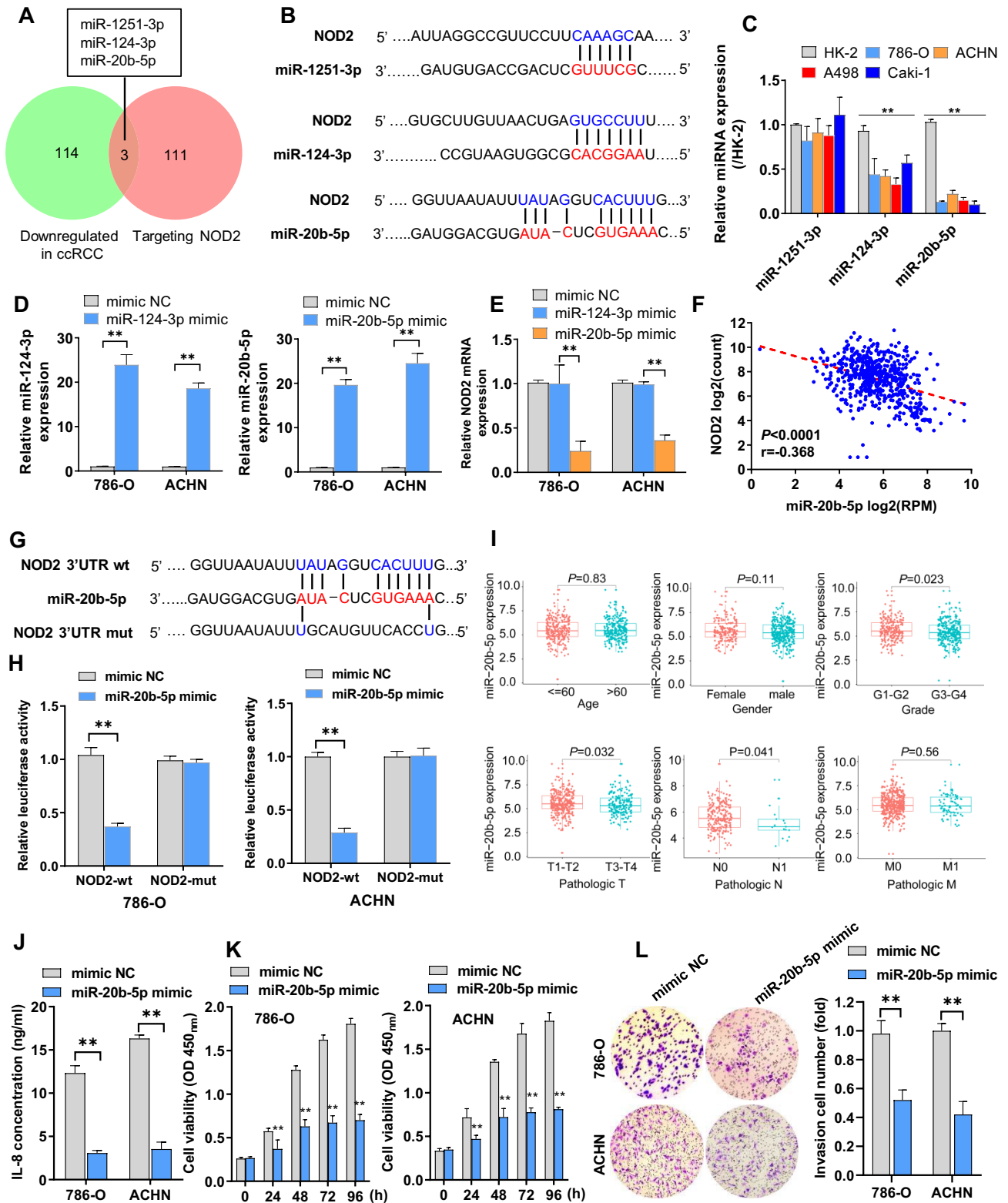
Discussion

Inflammation and immunity, the two important processes in the tumor microenvironment, influence tumor pathogenesis and progression. Inflammation-induced tumorigenesis is a complex process in which various cells, including T lymphocytes cells, B lymphocytes cells, macrophages, myeloid cells, fibroblasts and epithelial cells, interact with each other through membrane-associated molecular, matrix metalloproteases (MMPs) and soluble factors [18, 19]. Inflammation-related signaling pathways are involved in immune responses, in which a large number of immune-suppressive cells (such as regulatory T cell (Treg), tumor associated macrophages (TAM), myeloid-derived suppressor cells (MDSC)) and inflammatory factors (such as IL-6, IL-10, TNF- α , TGF- β) aggregate in the tumor microenvironment, resulting in tumor immune escape, growth and metastasis [20, 21]. Preoperative systemic immune-inflammatory indices can be used as important indicators for predicting tumor recurrence in ccRCC patients [22, 23]. However, the clinical value of IIRGs in the prognosis of ccRCC patients has not been fully established. Therefore, it is important to identify novel IIRGs and determine the associated mechanisms to improve ccRCC prevention and treatment.

In this study, through GSEA, we obtained 223 IIRGs and identified 59 upregulated IIRGs in the onset of ccRCC based on the TCGA database. These upregulated IIRGs were enriched in immune responses, cytokine and chemokine activities, toll-like receptor signaling pathway, NOD-like receptor signaling pathway as well as TNF signaling pathway. Then, we analyzed the correlation between upregulated IIRGs and prognostic outcomes for ccRCC patients.

It was established that ccRCC patients with elevated AIM2, CXCL13, JALK3, NOD2, PLCB2, PYCARD, TNIP3 and XCL2 levels had poor OS outcomes. However, among the eight prognostic-related IIRGs, only NOD2 and PYCARD were validated to be significantly upregulated in ccRCC. Given that NOD2 and PYCARD are potential clinical values of IIRGs for ccRCC, we explored the clinical significance of NOD2 and PYCARD and found that their expression levels were significantly positively correlated with tumor grade and pathological TNM stage. Moreover, cBioPortal analysis revealed that NOD2 and PYCARD mRNA expressions were significantly associated with alterations, mutations and methylation levels. Importantly, NOD2 and PYCARD levels were closely positively correlated with immune infiltrations.

NOD2 is a member of NOD-like receptor (NLR) family that participates in inflammatory responses and innate immune responses via NLR signaling, NF-kappa-B signaling and RIP2 signaling in the tumor microenvironment [24, 25]. In liver, breast, lung and colorectal cancers, NOD2 has been shown to play a dual role in tumorigenesis and progression [25–28]. Zhou et al. documented that NOD2, as a general intracellular pattern recognition receptor (PRR), promotes hepatocarcinogenesis via RIP-2 mediated pro-inflammatory responses [25]. Nashir Udden et al. reported that NOD2 suppresses colorectal inflammation as well as tumorigenesis by downregulating TLR-mediated activations of MAPK and NF-kappaB signaling pathways [28]. Liu et al. revealed that NOD2 polymorphisms are associated with increased cancer risk, including gastric cancer, MALT lymphoma and breast cancer [29]. PYCARD encodes an adaptor protein that is composed of 2 protein–protein interaction domains: an N-terminal PYRIN-PAAD-DAPIN domain (PYD) and a C-terminal CRAD [30]. PYDCRAD, as an inflammasome adaptor, is involved in cancer onset and development via inflammatory and apoptotic signaling pathways. Deswaerte et al. reported that PYCARD plays a pro-tumorigenic role in gastric cancer and suppresses cancer cell apoptosis via an IL-18 mediated inflammatory signaling pathway [31]. Liang et al. reported that PYCARD levels were significantly elevated in TMZ-resistant cell lines and glioma tissues, and that elevated PYCARD levels are independent risk factors for glioma prognosis [32]. A limited number of studies have elucidated the effects of NOD2 and PYCARD on ccRCC prognosis. Therefore, we investigated whether NOD2 and PYCARD are independent poor prognostic factors in ccRCC. The results showed that NOD2, but not PYCARD, is an independent unfavorable biomarker from conventional clinical variables (age, gender, tumor grade, pathological TNM stage), suggesting that expression of NOD2 influences the survival of ccRCC patients. Co-expression network analysis and GSEA showed that NOD2 may affected ccRCC progression and prognosis by regulating immune responses,



inflammatory responses, cytokine secretion and NF-kappaB signaling.

Given that NOD2 plays a crucial role in ccRCC tumorigenesis and progression, we investigated the potential

biological functions of NOD2 *in vitro*. The mRNA and protein levels of NOD2 in ccRCC cells were significantly elevated, compared to their expressions in human proximal tubular cells (HK2). Moreover, NOD2 knockdown

Fig. 7 Effects of miR-20b-5p on NOD2-induced ccRCC cell proliferation and invasion. **a** Overlapping prediction with miRDB, miRTarBase, TargetScan and Starbase databases showing the miRNAs that targeted NOD2. **b** Putative binding sites for miR-1251-3p, miR-124-3p and miR-20b-5p in the NOD2 3'-UTR sequence. **c** Expression levels of miR-1251-3p, miR-124-5p and miR-20b-5p in HK2 cells and four ccRCC cell lines (786-O, ACHN, A498 and Caki-1) were evaluated through qRT-PCR. $**P < 0.05$ vs. HK2 cells. **d, e** 786-O and ACHN cells were treated with miR-124-3p or miR-20b-5p for 24 h; mRNA expression levels of miR-124-3p, miR-20b-5p and NOD2 were determined by qRT-PCR. $**P < 0.05$ vs. mimic NC. **f** Pearson correlation analysis showing the correlation between NOD2 mRNA and miR-20b-5p levels. **g** Putative binding sites for miR-20b-5p in wild type/mutant NOD2 3'-UTR sequence. **h** Luciferase activity assay indicating the potential association between miR-20b-5p and NOD2 3'-UTR sequence. $**P < 0.05$ vs. mimic NC. **i** Relative expression of miR-20b-5p in subgroups of ccRCC samples stratified based on age, gender, tumor grade and pathological TNM stage. **j–l** 786-O and ACHN cells were treated with miR-20b-5p mimics and expression levels of IL-8, cell viability and cell invasion abilities were evaluated by ELISA, MTT and invasion assays, respectively. $**P < 0.05$ vs. mimic NC. In vitro experiment, data are representative images or expressed as the mean \pm SD of each group of cells from three independent experiments. Representative images are shown at $\times 100$ magnification

significantly inhibited ccRCC cell proliferation and invasion. Given that the progression of cancer is usually accompanied by the activation of inflammation, which is caused by increased secretion of inflammatory cytokines and activation of inflammatory pathways, we further explored the effect of NOD2 on the secretion of inflammatory cytokines in ccRCC cells. The results showed that IL-8 levels were significantly higher in ccRCC cells than in HK-2 cells. Silencing NOD2 suppressed IL-8 secretion and inhibited IL-8-induced invasion of ccRCC cells, suggesting that IL-8 secretion may be involved in progression of NOD2-related ccRCC. IL-8, also known as CXCL8, is a pro-inflammatory chemokine and a potent chemoattractant for myeloid leukocytes, which plays an important role in regulation of pathological processes of various inflammatory diseases and cancers [33]. Biologically, IL-8 enhances cancer cell proliferation and invasion via multiple mechanisms, including angiogenesis, epithelial mesenchymal transformation (EMT) and immunosuppression [34, 35]. Tumor-associated IL-8 is associated with poor outcomes following administration of immune checkpoint blockade therapy and serum IL-8 levels can predict the clinical benefits of PD-L1 blockade [36]. However, the precise mechanisms of NOD2-mediated secretion of IL-8 in ccRCC should be further explored.

miRNA biomarkers have important roles in cancer diagnosis and treatment [37, 38]. miRNAs are involved in post-transcriptional levels and bind the 3'-untranslated region (3'-UTR) of target mRNA, leading to inhibition or/and degradation of target mRNAs [39]. We found that miR-20b-5p was the potential miRNA that targets NOD2 and expression

levels of miR-20b-5p were significantly suppressed in both ccRCC tissues and cell lines. More important, bioinformatics analysis revealed that miR-20b-5p expression level was significantly negatively correlated with tumor grade and pathological TN stage, suggesting that low miR-20b-5p expression may be a risk factor for poor survival of ccRCC patients. Previous studies documented that miR-20b-5p is a tumor suppressor in various cancers [40–42]. Yang et al. reported that miR-20b-5p inhibits colon cancer proliferation, migration and invasion by targeting cyclin D1. Qi et al. found that miR-20b-5p suppresses prostate cancer migration and invasion by blocking TGF- β -induced EMT [41]. Liao et al. revealed that miR-20b-5p is a potential target of immune checkpoint gene CTLA4 in ccRCC [42]. Our study further indicated that miR-20b-5p inhibits ccRCC proliferation and invasion by blocking NOD2-mediated secretion activation of IL-8, suggesting that the miR-20b-5p/NOD2/IL-8 axis provides some novel insights into the molecular mechanisms of ccRCC and novel treatment targets.

Conclusions

In summary, we identified an IIRG, NOD2, from large ccRCC samples, to be a potential prognostic marker for ccRCC patients. Our findings also highlight the carcinogenic role of NOD2 in ccRCC. NOD2 promotes ccRCC cell proliferation and invasion by inducing IL-8 secretion. miR-20b-5p targets NOD2 to alleviate the NOD2-mediated IL-8 secretion, thereby inhibiting ccRCC cell proliferation and invasion. This finding demonstrates the regulatory mechanisms of NOD2 in ccRCC development. Further studies should be performed to determine the precise functions of NOD2 in the regulation of immune- and inflammation-mediated tumorigenesis in ccRCC.

Supplementary Information The online version contains supplementary material available at <https://doi.org/10.1007/s13577-024-01045-2>.

Author contributions Lei Lyu and Jingdong Yuan designed the experiments. Rui Min, Fuxin Zheng and Tao Huang performed the experiments. Lei Lyu and Tao Huang drafted the manuscript. Wei Xiang, Yan Feng and Chuanhua Zhang conducted data analysis and interpreted the results. Lei Lyu, Rui Min, Fuxin Zheng and Jingdong Yuan revised the manuscript. Lei Lyu, Rui Min and Fuxin Zheng contributed equally to this work as co-first authors. All authors reviewed and approved the manuscript.

Funding This study was supported in part by the National Natural Science Foundation of China (81902593, 82002708), Hubei Province Nature Science Foundation of China (2020CFB732, 2019CFB279) and Wuhan Science and Technology Project of China (2020020601012325).

Availability of data and materials The data used to support the findings of this study are available from the corresponding author upon request.

Declarations

Conflict of interest The authors declare no competing interests or conflict of interests.

Ethics approval and consent to participate This study was performed in line with the principles of the Declaration of Helsinki and was approved by the Ethics Committee of Wuhan No.1 Hospital, Tongji Medical College, Huazhong University of Science and Technology (Ethics Approval Number: 2020IECA255). Informed consent was obtained from all participating patients.

Consent for publication All authors gave consent for publication.

References

- Siegel RL, Miller KD, Jemal A. Cancer statistics, 2019. *CA Cancer J Clin.* 2019;69:7–34.
- Choueiri TK, Motzer RJ. Systemic therapy for metastatic renal-cell carcinoma. *N Engl J Med.* 2017;376:354–66.
- Capitanio U, Bensalah K, Bex A, Boorjian SA, Bray F, Coleman J, Gore JL, Sun M, Wood C, Russo P. Epidemiology of renal cell carcinoma. *Eur Urol.* 2019;75:74–84.
- Atkins MB, Tannir NM. Current and emerging therapies for first-line treatment of metastatic clear cell renal cell carcinoma. *Cancer Treat Rev.* 2018;70:127–37.
- Tacconi EMC, Tuthill M, Protheroe A. Review of adjuvant therapies in renal cell carcinoma: evidence to date. *Onco Targets Ther.* 2020;13:12301–16.
- Mattei J, da Silva RD, Sehrt D, Molina WR, Kim FJ. Targeted therapy in metastatic renal carcinoma. *Cancer Lett.* 2014;343:156–60.
- Lalani AA, McGregor BA, Albiges L, Choueiri TK, Motzer R, Powles T, Wood C, Bex A. Systemic treatment of metastatic clear cell renal cell carcinoma in 2018: current paradigms, use of immunotherapy, and future directions. *Eur Urol.* 2019;75:100–10.
- Dos Santos M, Brachet PE, Chevreau C, Joly F. Impact of targeted therapies in metastatic renal cell carcinoma on patient-reported outcomes: methodology of clinical trials and clinical benefit. *Cancer Treat Rev.* 2017;53:53–60.
- Flippot R, Escudier B, Albiges L. Immune checkpoint inhibitors: toward new paradigms in renal cell carcinoma. *Drugs.* 2018;78:1443–57.
- Diaz-Montero CM, Rini BI, Finke JH. The immunology of renal cell carcinoma. *Nat Rev Nephrol.* 2020;16:721–35.
- Motzer RJ, Tannir NM, McDermott DF, Aren Frontera O, Melichar B, Choueiri TK, Plimack ER, Barthelemy P, Porta C, George S, Powles T, Donskov F, Neiman V, et al. Nivolumab plus ipilimumab versus sunitinib in advanced renal-cell carcinoma. *N Engl J Med.* 2018;378:1277–90.
- Pan JH, Zhou H, Cooper L, Huang JL, Zhu SB, Zhao XX, Ding H, Pan YL, Rong L. LAYN is a prognostic biomarker and correlated with immune infiltrates in gastric and colon cancers. *Front Immunol.* 2019;10:6.
- Wang F, Cao X, Yin L, Wang Q, He Z. Identification of SCARA5 gene as a potential immune-related biomarker for triple-negative breast cancer by integrated analysis. *DNA Cell Biol.* 2020;39:1813–24.
- Koliaraki V, Prados A, Armaka M, Kollias G. The mesenchymal context in inflammation, immunity and cancer. *Nat Immunol.* 2020;21:974–82.
- Singh R, Mishra MK, Aggarwal H. Inflammation, immunity, and cancer. *Mediat Inflamm.* 2017;2017:6027305.
- Weber R, Groth C, Lasser S, Arkhypov I, Petrova V, Altevogt P, Utikal J, Umansky V. IL-6 as a major regulator of MDSC activity and possible target for cancer immunotherapy. *Cell Immunol.* 2021;359: 104254.
- Im JH, Buzzelli JN, Jones K, Franchini F, Gordon-Weeks A, Markelc B, Chen J, Kim J, Cao Y, Muschel RJ. FGF2 alters macrophage polarization, tumour immunity and growth and can be targeted during radiotherapy. *Nat Commun.* 2020;11:4064.
- Mantovani A, Ponzetta A, Inforzato A, Jaillon S. Innate immunity, inflammation and tumour progression: double-edged swords. *J Intern Med.* 2019;285:524–32.
- Pflug KM, Sitcheran R. Targeting NF-kappaB-inducing kinase (NIK) in immunity, inflammation, and cancer. *Int J Mol Sci.* 2020;21:8470.
- Liu Y, Li L, Li Y, Zhao X. Research progress on tumor-associated macrophages and inflammation in cervical cancer. *Biomed Res Int.* 2020;2020:6842963.
- Luoma AM, Suo S, Williams HL, Sharova T, Sullivan K, Manos M, Bowling P, Hodi FS, Rahma O, Sullivan RJ, Boland GM, Nowak JA, Dougan SK, et al. Molecular pathways of colon inflammation induced by cancer immunotherapy. *Cell.* 2020;182(655–71): e22.
- Fest J, Ruiter R, Mulder M, Groot Koerkamp B, Ikram MA, Stricker BH, van Eijck CHJ. The systemic immune-inflammation index is associated with an increased risk of incident cancer—a population-based cohort study. *Int J Cancer.* 2020;146:692–8.
- Huang H, Liu Q, Zhu L, Zhang Y, Lu X, Wu Y, Liu L. Prognostic value of preoperative systemic immune-inflammation index in patients with cervical cancer. *Sci Rep.* 2019;9:3284.
- Zhang L, Zhang B, Wei M, Xu Z, Kong W, Deng K, Xu X, Zhang L, Zetahao X, Yan L. TRIM22 inhibits endometrial cancer progression through the NOD2/NFkappaB signaling pathway and confers a favorable prognosis. *Int J Oncol.* 2020;56:1225–39.
- Zhou Y, Hu L, Tang W, Li D, Ma L, Liu H, Zhang S, Zhang X, Dong L, Shen X, Chen S, Xue R, Zhang S. Hepatic NOD2 promotes hepatocarcinogenesis via a RIP2-mediated proinflammatory response and a novel nuclear autophagy-mediated DNA damage mechanism. *J Hematol Oncol.* 2021;14:9.
- Velloso FJ, Sogayar MC, Correa RG. Expression and in vitro assessment of tumorigenicity for NOD1 and NOD2 receptors in breast cancer cell lines. *BMC Res Notes.* 2018;11:222.
- Wang Y, Miao Z, Qin X, Li B, Han Y. NOD2 deficiency confers a pro-tumorigenic macrophage phenotype to promote lung adenocarcinoma progression. *J Cell Mol Med.* 2021;25:7545–58.
- Udden SMN, Peng L, Gan JL, Shelton JM, Malter JS, Hooper LV, Zaki MH. NOD2 suppresses colorectal tumorigenesis via downregulation of the TLR pathways. *Cell Rep.* 2017;19:2756–70.
- Liu J, He C, Xu Q, Xing C, Yuan Y. NOD2 polymorphisms associated with cancer risk: a meta-analysis. *PLoS ONE.* 2014;9: e89340.
- Protti MP, De Monte L. Dual role of inflammasome adaptor ASC in cancer. *Front Cell Dev Biol.* 2020;8:40.
- Deswaerte V, Nguyen P, West A, Browning AF, Yu L, Ruwanpura SM, Balic J, Livis T, Girard C, Preaudet A, Oshima H, Fung KY, Tye H, et al. Inflammasome adaptor asc suppresses apoptosis of gastric cancer cells by an IL18-mediated inflammation-independent mechanism. *Cancer Res.* 2018;78:1293–307.
- Liang A, Zhong S, Xi B, Zhou C, Jiang X, Zhu R, Yang Y, Zhong L, Wan D. High expression of PYCARD is an independent predictor of unfavorable prognosis and chemotherapy resistance in glioma. *Ann Transl Med.* 2021;9:986.
- Alfaro C, Sanmamed MF, Rodriguez-Ruiz ME, Teijeira A, Onate C, Gonzalez A, Ponz M, Schalper KA, Perez-Gracia JL, Melero

- I. Interleukin-8 in cancer pathogenesis, treatment and follow-up. *Cancer Treat Rev.* 2017;60:24–31.
34. Gonzalez-Aparicio M, Alfaro C. Significance of the IL-8 pathway for immunotherapy. *Hum Vaccin Immunother.* 2020;16:2312–7.
 35. Ha H, Debnath B, Neamati N. Role of the CXCL8-CXCR1/2 axis in cancer and inflammatory diseases. *Theranostics.* 2017;7:1543–88.
 36. Yuen KC, Liu LF, Gupta V, Madireddi S, Keerthivasan S, Li C, Rishipathak D, Williams P, Kadel EE 3rd, Koeppe H, Chen YJ, Modrusan Z, Grogan JL, et al. High systemic and tumor-associated IL-8 correlates with reduced clinical benefit of PD-L1 blockade. *Nat Med.* 2020;26:693–8.
 37. Macfarlane LA, Murphy PR. MicroRNA: biogenesis, function and role in cancer. *Curr Genom.* 2010;11:537–61.
 38. Ali Syeda Z, Langden SSS, Munkhzul C, Lee M, Song SJ. Regulatory mechanism of MicroRNA expression in cancer. *Int J Mol Sci.* 2020;21:1723.
 39. Lewis BP, Burge CB, Bartel DP. Conserved seed pairing, often flanked by adenosines, indicates that thousands of human genes are microRNA targets. *Cell.* 2005;120:15–20.
 40. Qi JC, Yang Z, Zhang YP, Lu BS, Yin YW, Liu KL, Xue WY, Qu CB, Li W. miR-20b-5p, TGFBR2, and E2F1 form a regulatory loop to participate in epithelial to mesenchymal transition in prostate cancer. *Front Oncol.* 2019;9:1535.
 41. Yang H, Lin J, Jiang J, Ji J, Wang C, Zhang J. miR-20b-5p functions as tumor suppressor microRNA by targeting cyclinD1 in colon cancer. *Cell Cycle.* 2020;19:2939–54.
 42. Liao G, Wang P, Wang Y. Identification of the prognosis value and potential mechanism of immune checkpoints in renal clear cell carcinoma microenvironment. *Front Oncol.* 2021;11:720125.

Publisher's Note Springer Nature remains neutral with regard to jurisdictional claims in published maps and institutional affiliations.

Springer Nature or its licensor (e.g. a society or other partner) holds exclusive rights to this article under a publishing agreement with the author(s) or other rightsholder(s); author self-archiving of the accepted manuscript version of this article is solely governed by the terms of such publishing agreement and applicable law.